Title

The Hydrogen Molecule under the Reaction Microscope:
Single Photon Double Ionization at maximum Cross Section and Threshold (Doubly Differential Cross Sections)

Authors

Thorsten Weber[1], Lutz Foucar[2], Till Jahnke[2], Markus Schoeffler[2], Lothar Schmidt[2], Michael Prior[1], and Reinhard Doerner[2]

[1] Chemical Sciences Division, Lawrence Berkeley National Laboratory, Berkeley, CA 94720, USA
[2] Institut fuer Kernphysik, Goethe-Universitaet, Max-von-Laue-Str.1, 60438 Frankfurt am Main, Germany

Abstract

We studied the photo double ionization of hydrogen molecules in the threshold region (50 eV) and the complete photo fragmentation of deuterium molecules at maximum cross section (75 eV) with single photons (linearly polarized) from the Advanced Light Source, using the reaction microscope imaging technique. The 3D-momentum vectors of two recoiling ions and up to two electrons were measured in coincidence. We present the kinetic energy sharing between the electrons and ions, the relative electron momenta, the azimuthal, and polar angular distributions of the electrons in the body fixed frame. We also present the dependency of the kinetic energy release in the Coulomb explosion of the two nuclei on the electron emission patterns. We find that the electronic emission in the body-fixed frame is strongly influenced by the orientation of the molecular axis to the polarization vector and the internuclear distance as well as the electronic energy sharing. Traces of a possible breakdown of the Born-Oppenheimer approximation are observed near threshold.

Introduction

The investigation of correlated many-body systems is a key challenge in many fields of physics, chemistry, and microbiology. The correlated motion of electrons and ions determines major physical effects in solid-state physics, atomic and molecular phenomena, and nuclear reactions. However, after more than a century, quantum theory has not offered an analytic solution for the wave function of any physical system with three or more charged particles. Within the past three decades many theoretical [1 - 15] and experimental [16 - 36] investigations of the photo double ionization (PDI) of helium atoms became a testbed for the investigation of a fundamental atomic three-body problem. Following many technical innovations this research has led to a detailed description of the important dynamics in this system.

On the experimental side reaction microscopy, employing time and position sensitive detectors [37, 38], has enabled substantial breakthroughs because it often delivers fully differential cross sections. Based on a coincidence electron-ion 3D-momentum imaging technique, the kinematics of the ionization process can be displayed in internal (electron-electron) frames. In some cases kinematically complete experiments, i.e. the full coincident detection of the 3D-momenta of all particles involved and covering the entire final state phase space (apart from spin orientations), have been realized (e.g. [21]). Despite this progress, taking the next step, i.e. understanding the complete fragmentation of molecular hydrogen with a single photon, remains a fundamental and challenging four-body-problem.

Early work in theory [39 - 43] and experiment [44 - 48] laid the foundation over 30 years ago, but even the more modern theoretical approaches [49 - 57] and measurements [58 - 69] struggle to paint the full picture. In the photon energy regime of the latter studies the momentum of the photon is almost negligible compared to the momenta of the massive fragments. Accordingly, the absorption of light is almost equivalent with the deposition of pure energy accompanied by one unit of angular momentum into the molecular system. While angular momentum and parity accounting must be followed, the angular momentum of the electronic subsystem is not a conserved quantity in the two center Coulomb potential.

Moreover, depending on the photon wavelength, four additional aspects in this PDI process are relevant and can be categorized as follows (Compton scattering, which becomes relevant at very high photon energies and drew a lot of attention in the PDI of He [70 - 73], is not considered here):

a. the finite internuclear distance and the relative-momentum vector of the recoiling ions define new

coordinate frames, which break the radial symmetry of the initial and final state. The molecular symmetries yield a distinct influence on the angular distributions of the electrons with respect to the molecular orientation.

b. the exchange of angular momentum between the electrons and the molecular axis affects the dynamics of the final state.
c. for photon energies producing short electron wavelengths in the continuum comparable to the internuclear distance, the two-center-geometry of the protons represents a molecular double-slit for the outgoing electron pair. Young-type interference effects can accompany the diffraction-pattern.
d. the dynamics of the four-particle motion, i.e. the interplay of two correlated electrons and two recoiling nuclei, triggered by the PDI and subsequent molecular breakup, governs the relative particle emission patterns. In most cases the ionization process is described within the Born-Oppenheimer approximation, which typically does not include any interaction of the emitted electron(s) and the final ionic state. This approximation might be violated when the electron energy is low enough, because in that case the electrons and ions move on the same timescales and possibly interact with each other.

Points (a) and (b), which are constrained by various kinematic selection rules [74 - 76], were experimentally successfully revealed by highly differential cross sections measurements [61, 62, 63, 65] and these measurements stimulated intricate numerical solutions of the Schrödinger equation (see e.g. [49, 50, 51]). Strong influences of the ion kinetic energy release (KER) on the electron emission patterns were found. An even stronger KER sensitivity was found for the single ionization of H_2 with subsequent dissociation. In this case selecting different KERs revealed strong asymmetries in the associated molecular frame photo electron angular distributions as final states with σ and π symmetries were coherently mixed [77, 78].

Issues (c) and (d) are both very challenging to study experimentally. This is because in both cases, the cross sections are very low, while at the same time a coincident (multi-hit) detection of electron and ion pairs is required. Thus the experimental event rate is very low even when using 4π imaging detection systems. However, by improving the momentum resolution of the ion detection scheme in modern reaction microscopes, the 3D-momentum vector of the fast electron could be derived from the momenta of the two recoiling ions and the slow electron via the momentum conservation law. This approach reduces the number of particles to be collected in coincidence inside the spectrometer from four to three, i.e. two recoiling ions and one electron. This is very beneficial for gathering statistically meaningful results in a reasonable time. It enabled kinematically complete measurements of the PDI of H_2 at photon energies of 160 eV and higher. Molecular T. Young double slit experiments could be performed studying interference effects and electron-electron entanglement [64, 66, 67, 68]. Moreover, this technical advancement has been applied successfully to study the PDI of more complex molecules such as N_2 [79 - 83] and C_2H_4 [84], where similar effects were observed.

However, the experimental investigation of the PDI near threshold [(d) above] remains highly demanding. This is because the small electron momenta cannot be resolved from a measurement of the ion momenta, which are dominated by the ionic Coulomb repulsion. But it is exactly here where four body dynamics (i.e. point d) is expected to be at its strongest. Once the electrons are in the same velocity range as the recoiling ions, the Coulomb interactions will cause a breakdown of the Born-Oppenheimer approximation. Such electrons can even retroact. This was for instance observed in the single ionization and subsequent dissociation of H_2 [85]. In this case the proton trajectory is influenced by the presence of the long-range Coulomb potential of the retroacting electron.

Investigating the final state of the PDI of a hydrogen molecule is equivalent to the observation of an unbound four-body Coulomb system with no molecular degrees of freedom. This system will display the correlated motion of all its constituents since the energy of the ionizing photon must be shared by all the outgoing particles. Two electrons excited into the continuum near the ionization threshold can offer unique insight into the nature of electron correlation. Electron-electron correlation is omnipresent in nature and is responsible for important effects such as superconductivity and the quantized fractional Hall Effect and many others. Hence, the investigation of the PDI of H_2 in the threshold region is of fundamental interest and demands further study.

Of particular interest is the electron ejection pattern of this molecular break-up, as its structure is a reflection of four different interplays, which are affected by several constraints. We have to contemplate

1.) Electron-electron correlation as determined by the initial two-electron wavefunction
2.) Electron-electron repulsion and selection rules based on parity and angular momentum conservation depending on the energy sharing of the two electrons
3.) Electron-nuclei interaction, influenced by symmetry effects of the molecular state as well as selection rules due to parity and angular momentum conservation
4.) Nuclei-nuclei repulsion, restrained by total energy conservation and the correlated initial wavefunction

Referring to the latter (i.e. point 4), the two electrons are ejected instantaneously from a molecule with the nuclei at a certain internuclear distance. This distance is governed by the zero-point motion of the nuclei in the molecular ground state. Subsequently, the two nuclei separate with a kinetic energy determined by the potential energy of their coulombic repulsion at the internuclear distance the photon was absorbed. The kinetic energy distribution of the repelling nuclei has a width of FWHM= 4.5 eV and is quite broad. This corresponds to internuclear distances of 0.6 to 0.9 Å for a hydrogen molecule, resulting in an average ion energy of around 9.4 eV. Therefore, no sharp double ionization threshold, as in the atomic case, can be observed.

The ionization potential of 31.6 eV represents the sum of the binding energy of each electron in a hydrogen atom ($2 \cdot 13.6$ eV) plus the dissociation energy of the neutral H_2 molecule (4.52 eV). A mean value of the PDI region is then given by $2 \cdot 13.6 + 4.52 + 2 \cdot 9.4 = 50.52$ eV. In the experiment presented here, a photon energy of 50 eV was chosen to investigate the behavior in the threshold region and compare it to the PDI at 75 eV. The latter photon energy corresponds to the double ionization of H_2 at around its maximum cross section [39, 40]. For a fixed photon energy the ionization process at different internuclear distances changes the kinetic energy available to be shared by the outgoing electrons due to energy conservation. Moreover, different bondlenghts of the ground state of the molecule result in different initial electronic wavefunctions.

In most cases of the PDI, even in the threshold region, the Born-Oppenheimer approximation is appropriate. For a hydrogen molecule, an electron energy of 5 meV and lower is required for similar velocities to the recoiling ions resulting in a possible breakdown of this model. Since the cross section for photo double ionization of hydrogen molecules at 50 eV is lower than $1 \cdot 10^{-21}$ cm^2, a coincident observation of all four particles is very difficult. Moreover, because both ejected electrons are very similar in energy, the difference in their times-of-flight to one common detector is evanescent. As a result current multi-hit particle detection limitations of 3D-momentum spectroscopy, which relies on time-of-flight measurements, are problematic. Resolving electron energies below 100 meV is challenging for any experimental set-up. Therefore it is very difficult to make progress in the region of possible strong non-Born-Oppenheimer behavior using current experimental methods.

Nevertheless, especially in comparison with the PDI at maximum cross section (75 eV), the fragmentation at threshold can help to answer the question whether the ejection pattern of the electrons, which varies with the internuclear distance [49, 50, 51, 62, 65], reflects a purely kinematic effect, or if it is due to changes in electron correlation of the initial state wave function. Hence, in the following sections the break-up of hydrogen molecules close to threshold (50 eV) and deuterium molecules at maximum cross section (75 eV), investigated with the reaction microscope technique, will be presented. To our knowledge no highly differential theoretical investigation of the PDI of H_2 in the threshold region, which could complement the experimental data, exists yet. The results presented here may stimulate the intricate quantum mechanical calculations needed for this challenging threshold region.

Technique

By fragmenting an atomic or molecular quantum system many of its initial properties like bond angles, symmetries etc. become observable. As it turns out, in the majority of cases, the main information is hidden in the 3D-momentum distributions of the outgoing electrons with respect to a specified direction

of the system. This quantization axis can be for instance the photon polarization or the molecular axis. In order to examine these emission patterns, a device is needed that visualizes the trajectories of all particles in the fragmentation process of the target upon photon absorption. Once all 3D-momentum vectors of the outcome are obtained, highly differential cross sections reveal the information of the correlated motion of the many-body system.

A so called reaction microscope has been used to detect electrons and ions in coincidence for each photo double ionization event. Detailed information about the technique, which is also called COLd Target Recoil Ion Momentum Spectroscopy (COLTRIMS), can be found elsewhere [86 - 88]. In brief, in this setup the pulsed linearly polarized photon beam (with a pulse duration of 80 ps) of 50 eV energy, provided by beamline 10.0.1 of the Advanced Light Source synchrotron ring of the Lawrence Berkeley National Laboratory, is intersected with an internally cold and well-localized supersonic gas jet under 90 degrees inside the momentum spectrometer. The PDI of deuterium molecules at maximum cross section (75 eV) was investigated at beamline 7.0.1 employing the same approach.

In this imaging scheme the electrons and ions are guided by parallel homogenous electric and magnetic fields towards two opposite large position sensitive multi-channel plate detectors. Each of them are equipped with fast delay-line readout anodes. They are capable of handling multiple particle hits from each event within certain limitations; a deadtime of ~5 ns remains for hits that are less than ~5 mm apart [38, 89]. The fields are chosen such that a solid angle of detection of 4π is achieved for the electrons and ions at the same time. For each particle the 3D-momentum vector can then be deduced from the measured time-of-flight and the two dimensional position of impact on the respective detector. Since the raw data is recorded without restrictions, it is possible to extract all information of interest offline at a later time. The intricate offline analysis allows the transformation of the multidimensional momentum phase space to any desired coordinate frame most appropriate for the physical process under investigation.

Applying the axial-recoil-approximation [90, 91], the COLTRIMS technique enables us to determine the orientation of the molecular axis at the time of the photoionization event. This is because the momentum vectors of the recoiling ions in the final state are measured. From the KER of the recoiling ions and by applying the reflection approximation to the potential energy curves, the internuclear distance at the instant of photoionization can then be derived.

In cases where the Born-Oppenheimer approximation is inadequate, the axial-recoil-approximation will be compromised as well. The angular electron distributions in the body-fixed frame are then expected to wash out. The final state momenta of the ions do not represent the orientation of the molecular axis at the time of photon absorption anymore (compare to [92 - 94]). However, due to strong multi-hit detection challenges and the very small cross section, for most of the results shown here, only one electron in coincidence with two protons were detected for the PDI in the threshold region. Hence, mostly Doubly Differential Cross Sections DDCSs will be presented here.

Results

The PDI events were filtered out during the offline analysis by requiring the two detected recoiling ions to have a sum momentum close to zero. This is a fingerprint of two ions being emitted back-to-back in a Coulomb explosion, as it takes place after a direct photo double ionization of H_2. Using these filtered data the following magnitudes are plotted to shine light on the dynamics of the fragmentation process:

Energy map

In Figure 1 the kinetic energy of one electron as a function of the KER of the recoiling ions exhibits the accessible energy phase space of the reaction for a photon energy of 75 eV (Fig. 1a) and 50 eV (Fig. 1b). The solid white diagonal line indicates the maximum allowed kinetic energy of all four particles requiring the second electron to have a vanishing value. While for the higher photon energy (75 eV) the electron energy is independent of the KER in about 80 percent of the cases, the electron energy is highly constrained by total energy conservation at $E_\gamma = 50$ eV. Thus, only for very low energy electrons (below 1 eV) the KER covers the full possible range of the Franck-Condon region. Alternatively, the truncation in final state phase space for the electrons apparently limits the ionic energies to lower values. Thus, only electrons with energies below 1 eV were chosen for some of the polar angular distributions at 50 eV (i.e.

Figure 3 and 8 below) in order to eliminate effects due to a constricted phase space by the KER.

Azimuthal angles

For the case of a photon energy of 50 eV we restricted the investigation to a KER interval in Figure 2a-c ranging from 12 to 16 eV. This represents a hydrogen molecule with a large internuclear distance. It allows us to investigate the angular distribution of the emitted electron perpendicular to the polarization vector for the complete available interval of electron kinetic energies (0 to 4 eV). In this so called azimuthal plane the molecular axis is aligned horizontally, while the polarization vector is orientated normal to this plane. For comparison the angular distribution for a photon energy at 75 eV with a similar cut in KER (12 to 18 eV) is presented in Figure 2d-f.

The sequence of spectra shows that low energy electrons, which are generated at 50 eV, are slightly more aligned along the molecular axis. For electrons with higher energy the distribution becomes more isotropic. However, a circular shape like for the PDI of helium atoms is not reached, even when the smallest internuclear distances (resp. a large KER) are chosen (not shown here: it resembles Figure 2f). This slight effect is true for both photon energies used here (50 and 75 eV) but contrasts observations at 58 eV [58], which found this distribution to be circular. This might be interpreted as a stronger electron-nuclei interaction for lower energy electrons due to non-Born-Oppenheimer effects, but no theoretical proof for this assumption can be given here. However, even without violating the Born-Oppenheimer approximation, such an effect might be explainable by the increased sensitivity of the low energy electrons to the anisotropy of the two center field of the nuclei.

Polar angles

In Figure 3a-f a coplanar geometry is chosen to present the polar angular distributions for low energy electrons (0 to 1 eV) produced by 50 eV photons. In this geometry the Jacobi coordinate k_- for the recoiling ions was calculated as $k_-=(k_1-k_2)/2$ (representing the molecular axis) and applied to span a plane with the polarization vector ε of the incoming linearly polarized light. While integrating over the emission direction of one electron, events are chosen with the depicted second electron to be in this plane with an acceptance angle of ±20 degree. The sequence in Figure 3 shows the electronic angular distribution for different orientations of the molecular axis with respect to the horizontal polarization vector ε (5, 10, 15, 20, 55 and 90 degree).

The spectra in Figures 3a to 3e resemble a superposition of two 2-lobes-structures mirrored along the molecular axis with a rising emission probability for larger angles of the molecular axis with respect to the polarization vector. It is strongest for a perpendicular molecular orientation to the polarization vector, due to the solid angle. Starting with a d-wave like shape of the angular distribution for pure Σ-Σ-transition (which is due to selection rules but not shown here) the electron angular distributions become asymmetric such that the plotted electron is emitted preferably perpendicular to the molecular axis. This is true for molecular orientations below 25 degrees with respect to the polarization axis. With an increasing contribution of the final states with Π-symmetry, i.e. rising angle of the molecular axis, the electron emission follows the orientation of the molecule.
While for a pure Σ-Π-transition (Figure 3f) parity conservation requires a p-wave like shape, this evolution is a function of the electronic energy sharing. This becomes evident in comparison with the doubly differential cross sections obtained in the PDI at 75 eV. These results are shown in Figure 4a-f for electrons with an energy of 0 to 3 eV, in Figure 5a-f for electrons with 11 to 14 eV, and Figure 6a-f for electrons ranging from 19.5 to 30 eV.

There is a noticeable resemblance between Figure 3 and 5, i.e. the differential cross sections for two different photon energies. This is likely due to the fact that in both cases the electronic energy sharing is almost equal. For low energy electrons, produced by photons with 75 eV energy (see Figure 4a-d), the angular distribution for final states with mainly Σ-symmetry shows a more structured shape (resembling an f-wave) and a tendency for electrons to be emitted perpendicular to the polarization vector. For angles of the molecular axis bigger than 30 degrees (Figure 4e+f) the electrons behave like in Figure 3 and 5. High energy electrons show a different behavior (see Figure 6a-e). Starting also with a sharp d-wave like shape for a pure Σ-Σ-transition (not shown here), the distribution evolves such that a node along the

molecular axis is visible. For molecular orientations below 30 degree with respect to the polarization vector, the emission patterns represent almost the mirror image of the low electron energy case (Figure 3a-d and 4a-d) and the scenario of equal electron energy sharing (Figure 5a-d), while Figure 6d shows a preferred electron emission, which resembles the opposite pattern of Figures 3d, 4d and 5d.

Relative electron momenta

In Figure 7 the internal relative momenta of the two emitted electrons are presented for the PDI of H_2 at 50 eV. These spectra are based on rare four-particle coincidences recorded at this low photon energy. The filtered data require two recoiling protons to clearly identify the fragmentation process and two electrons, which are depicted here. The rather poor statistics is due to the experimental multi-hit particle detection problem, the small detection efficiency for four particles, i.e. two electrons and two recoiling protons, and the very low PDI cross section at threshold. The data were derived from a parallel data recording scheme based on fast flash-Analog to Digital Converters and a complex offline double pulse Gaussian fit routine, applied to all raw signal traces of the electron (Multi Channel Plate) detector (with hexagonal delay-line readout) [38, 89]. This way of data recording can be up to a factor of ~20 more efficient in the relevant phase space but was limited to acquisition rates of 1 kHz only, at the time the measurement was performed.

An internal electron-electron plane is spanned by the two electrons with one of them being emitted always to the right, as indicated by the arrow while its length has no meaning. The maximum possible momentum of the depicted electron is normalized to 1 for better comparison of the three cases, which differ in their electron sum energy. I.e. the case where the depicted electron carries all the excess energy and the other electron has zero energy corresponds to a circle with a radius of 1. The other inner black circle indicates equal energy sharing. The electron sum energy was limited from (A) 0 to 1eV, (B) 1 to 2 eV, and (C) 2 to 3 eV. All three cases are integrated over the orientation of the polarization vector and the molecular axis. The mean angle between the electrons is indicated by the diagonals. They show that the relative angle between the two emitted electrons is 132.07 degree in (A), 131.41 degree in (B), and 130.16 degree in (C), which reflects that the relative angle decreases for an increasing electron sum energy. For decreasing excess energy the electrons are more and more emitted back-to-back. This is a direct consequence of electron-electron repulsion, becoming increasingly important for slower electrons. This finding is in line with previous observations where, for the case of equal energy sharing, the fully differential cross sections are purely given by the width and amplitude of a Gaussian distribution. This is because the differential cross section can be parameterized [21] as:

$$\frac{d^4\sigma}{dE_1 d\cos\theta_1\, d\cos\theta_2\, d\varphi} \propto \left|(\cos\theta_1 + \cos\theta_2)a_g(E_1,\theta_{12}) + (\cos\theta_1 - \cos\theta_2)a_u(E_1,\theta_{12})\right|^2$$

with θ_1 and θ_2 being the polar angles of the two electrons 1 and 2 with respect to the polarization vector, θ_{12} the relative polar angle between the two electrons, φ the azimuthal electron angle, a_g and a_u being complex amplitudes, and E_1 the kinetic energy of electron 1. Since a_u is antisymmetric in terms of exchanging the particle numbering, it can be shown that $a_u = 0$ for equal energy, which leaves a_g the complex amplitude to describe the differential cross section. It is commonly expressed by:

$$\left|a_g(\theta_{12})\right|^2 = Ae^{\left(-(\theta_{12}-180)^2/2\sigma_w\right)}$$

with A being the amplitude and σ_w the width of the Gaussian distribution.

Since the electron sum energy is very small for the case of the near threshold double ionization, the two electron energies can be treated as almost equal. Hence, the above parametrization is expected to be applicable. It has been observed that the width of the Gaussian distribution is actually narrower for hydrogen molecules (see [46, 47, 48, 100] and 89.7°±2 FWHM found in this work at 24.5 eV excess energy in the 75 eV measurement) than for helium atoms [21, 23, 95, 96, 97, 98, 99]. As in those past experiments the distribution decreases with decreasing electron sum energy, as observed here as well for an ionization energy of 50 eV. However, due to the poor statistics, the angular distributions cannot be generated and hence the Gaussian fits to the differential cross sections at 50 eV cannot be derived.

KER-effects

In Figures 8 to 11 the polar angular distributions of one electron for three different KERs are presented, while the orientation of the molecular axis is fixed to 45 degrees with respect to the polarization vector ε of the incoming light. Figure 8 depicts the evolution for a fragmentation of H_2 in the threshold region (50 eV) for low energy electrons (0 to 1 eV). For small KER or large internuclear distances respectively (Fig. 8a) the body-fixed angular distribution shows a preferred emission along the molecular axis. This behavior is changing once bigger KERs or smaller internuclear distances are chosen (see Fig. 8a+b). Finally, a highly structured electron emission pattern, which is created by contributions from higher angular momenta, is shown in Fig. 8c. Apparently, the kinetic energy of the electrons plays an important role in this scenario as seen in the complementing spectra (Figures 9 to 11) for the PDI of D_2 at 75 eV. Choosing similar KER intervals at this higher photon energy, electrons with 0 to 5 eV are shown in Figure 9a-c, 10 to 15 eV are presented in Figure 10a-c, and 19.5 to 35 eV can be seen in Figure 11a-c. While increasing the electron energy, a preferred emission of the electron along and perpendicular to the polarization vector becomes apparent, filling up a minimum in the angular distribution (compare Figures 8a, 9a, 10a, and 11a).

Moreover, the ratio between these two emission probabilities changes with the KER (see Figures 11a-c). For high KER or small molecular bondlengths a fast electron is emitted preferably along the polarization vector ε of the incoming light, suggesting only one electron to contribute to the emission distribution. However, the presence of the second electron in the process of the PDI is evident in the still noticeable emission probability along the direction perpendicular to the polarization vector ε. Multi Scattering theory in Non Spherical self-consistent Potentials (MSNSP) [101] for the single ionization of H_2^+ (not shown here) describes a pure *p*-wave exhibiting a sharp minimum at 90 degrees.

Summary

We studied the PDI of hydrogen molecules near threshold and the complete fragmentation of deuterium molecules at maximum cross section with single photons (linearly polarized light). The focus of this research was on the investigation of the dynamics of four-particle motion in the final state and especially on hints for a breakdown of the Born-Oppenheimer approximation, which ultimately depends on the photon energy. The electron-ion energy correlation map revealed the different amount of independent phase space available in the final state of the reaction for the two different photon energies of 50 and 75 eV, emphasizing a smaller Franck-Condon-region and the strong dependence of the kinetic electron energies on the KER for the PDI at threshold.

While integrating over one electron, 50 eV and 75 eV photons were chosen to compare the emission patterns of the second electron with respect to the molecular axis. The azimuthal electron angular distributions at 50 eV exhibits a preferred emission along the molecular axis for low energy electrons, hinting electron-nuclei interaction and a possible violation of the Born-Oppenheimer approximation for a fraction of the PDI processes.

The polar angular distribution of the electrons in the body-fixed frame revealed a strong influence of the electronic emission pattern on the orientation of the molecular axis. Since even the lowest electron energy presented here still is a 100 times larger than the necessary kinetic energy for the electrons to be in comparable velocity ranges as the recoiling ions, no dramatic break-down of the Born-Oppenheimer approximation could be expected and observed. However, the relative emission angle between the two electrons is slightly increasing with a decreasing electron sum energy. I.e. the emission pattern indeed changes with the velocity of the electrons for all orientations of the molecular axis and the polarization vector as predicted in the literature. Nevertheless, as can be derived from the sequence of different molecular orientations, the electronic polar angular distributions are mainly dominated by electron-electron interaction, symmetry effects, and selection rules. Hence, for the low photon energy at hand (50 eV), the electronic energy sharing is more important than the absolute value of the kinetic energy: electrons with similar energy sharing at 50 and 75 eV show the same trend in the angular distribution along and perpendicular to the molecular axis, while low energy electrons at 75 eV exhibit a contribution of emissions perpendicular to the polarization vector. This behavior is true for orientations of the molecular axis below 45 degrees with respect to the linear polarization of the incoming light: once the final states yield more

Π-symmetry the emission patterns look the same. On the other hand, for high energy electrons (>19 eV) the kinematics is almost reversed.

The investigation of the KER dependency on the polar angular distribution for a fixed molecular orientation (45 degrees) reveals the interplay of electron-electron interaction, electron-nuclei interaction, and the influence of the initial state wave function. While for low energy electrons and large internuclear distances a preferred emission along the molecular axis is evident, a highly structured electronic angular distribution can be observed for small molecules. When the electron energy is increasing, the electron emission is preferably aligned along the polarization vector of the incoming light. The remaining contributions of electrons emitted perpendicular to the polarization vector indicate the presence of the second electron.

While the experimental observations and the comparison of the results of the two photon energies show a high level of detail, a theoretical explanation is missing due to the complexity of the four-body problem, which requires intricate computations. Especially the investigation of possible non Born-Oppenheimer effects in the threshold region of the PDI of H_2 remains challenging. Until ab-initio calculations become available, helium-like models, describing the emission of electron pairs into the continuum, may be an economic route to pursue [102]. We hope the presented doubly differential cross sections will stimulate computations of any kind to illuminate the dynamics and kinematics of this fundamental four-body problem.

Acknowledgement

Work at LBNL was performed under the auspices of the U.S. Department of Energy (DOE) under Contract No. DEAC02-05CH11231, using the Advanced Light Source (ALS) and National Energy Research Computing Center (NERSC), and was supported by the ALS U.S. DOE Office of Basic Energy Sciences, Division of Chemical Sciences. We thank the staff of the Advanced Light Source, in particular beamline 10.0.1 and 7.0.1 scientists for their outstanding support. We acknowledge the financial support of the Deutsche Akademische Austausch Dienst (DAAD) and the Deutsche Forschungs Gemeinschaft (DFG) as well as the Bundes Ministerium fuer Bildung und Forschung (BMBF). We are indebted to the RoentDek Company for long-term support with detector software and hardware.

References

1. M. Brauner, J.S. Briggs und H. Klar, J. Phys. B: At. Mol. Opt. Phys., **22**, (1989), 2265-2287
2. I. Bray und A.T. Stelbovics, Phys. Rev. A, **46**, (1992), 6995−7011
3. F. Maulbetsch und J.S. Briggs, J. Phys. B: At. Mol. Opt. Phys., **26**, (1993), 1679
4. F. Maulbetsch and J. S. Briggs, (1993), J. Phys. B: At. Mol. Opt. Phys., **26**, L647
5. D. Proulx und R. Shakeshaft, Phys. Rev. A, **48**, (1993), R875
6. F. Maulbetsch und J.S. Briggs, J. Phys. B: At. Mol. Opt. Phys., **27**, (1994), 4095
7. M. Pont und R. Shakeshaft, Phys. Rev. A, **51**, (1995), R2676
8. D.V. Fursa und I. Bray, Phys. Rev. A, **52**, (1995), 1279
9. M. Pont, R. Shakeshaft, F. Maulbetsch und J.S. Briggs, Phys. Rev. A, **53**, (1996), R3671
10. A.S. Kheifets und I. Bray, Phys. Rev. A, **54**, (1996), R995−R998
11. D.V. Fursa und I. Bray, J. Phys. B: At. Mol. Opt. Phys., **30**, (1997), 757
12. A.S. Kheifets und I. Bray, Phys. Rev. A, **57**, (1998), 2590−2595
13. A.S. Kheifets und I. Bray, J. Phys. B: At. Mol. Opt. Phys., **31**, (1998), L447−L453
14. J.S. Briggs und V. Schmidt, J. Phys. B: At. Mol. Opt. Phys., **33**, (2000), Topical Review, R1- R48
15. M. Walter, J.S. Briggs und J.M. Feagin, J. Phys. B: At. Mol. Opt. Phys., **33**, (2000), 2907-2927

16. O. Schwarzkopf, B. Krässig, J. Elmiger und V. Schmidt, Phys. Rev. Lett, **70**, (1993), 3008

17. R. Dörner, T. Vogt, V. Mergel, H. Khemliche, S. Kravis, C.L. Cocke, J. Ullrich, M. Unverzagt, L. Spielberger, M. Damrau, O. Jagutzki, I. Ali, B. Weaver, K. Ullmann, C.C. Hsu, M. Jung, E.P. Kanter, B. Sonntag, M.H. Prior, E. Rotenberg, J. Denlinger, T. Warwick, S.T. Manson, H. Schmidt-Böcking, (1996), Physical Review Letters, **76**, 2654

18. H. Bräuning, R. Dörner, C.L. Cocke, M.H. Prior, B. Krässig, A. Bräuning-Demian, K. Carnes, S. Dreuil, V. Mergel, P. Richard, J. Ullrich, H. Schmidt-Böcking, (1997), J. Phys. B: At. Mol. Opt. Phys., **30**, L649

19. H. Bräuning, R. Dörner, C.L. Cocke, M.H. Prior, B. Krässig, A.S. Kheifets, I. Bray, A. Bräuning-Demian, K. Carnes, S. Dreuil, V. Mergel, P. Richard, J. Ullrich, H. Schmidt-Böcking, (1998), J. Phys. B: At. Mol. Opt. Phys., **31,** 5149

20. R. Dörner, J. Feagin, C.L. Cocke, H. Bräuning, O. Jagutzki, M. Jung, E.P. Kanter, H. Khemliche, S. Kravis, V. Mergel, M.H. Prior, H. Schmidt-Böcking, L. Spielberger, J. Ullrich, M. Unverzagt, T. Vogt, (1996), Physical Review Letters, **77**, 1024

21. R. Dörner, H. Bräuning, J. Feagin, V. Mergel, O. Jagutzki, L. Spielberger, T. Vogt, H. Khemliche, M.H. Prior, J. Ullrich, C.L. Cocke, H. Schmidt-Böcking, (1998), Phys. Rev. A, **57**, 1074

22. J. S. Briggs and V. Schmidt, (2000), J. Phys. B: At. Mol. Opt. Phys., **33**, R1

23. S. Cvejanovic, J.P. Wightman, T.J. Reddish, F. Maulbetsch, M.A. MacDonald, A.S. Kheifets and I. Bray, (2000), J. Phys. B: At. Mol. Opt. Phys., **33**, 265 – 283

24. M. Achler, V. Mergel, L. Spielberger, R. Dörner, Y. Azuma, H. Schmidt-Böcking, (2001), J. Phys. B: At. Mol. Opt. Phys., **34**, 965 - 981

25. H. Schmidt-Böcking, V. Mergel, R. Dörner, H. Bräuning, M. Achler, L. Spielberger, O. Jagutzki, Th. Weber, Kh. Khayyat, J. Ullrich, C.L. Cocke, M.H. Prior, Y. Azuma, Y. Awaya, T. Kambara, (1999), Australian Journal of Physics, **52**, 523 – 535

26. Th. Weber, M. Weckenbrock, A. Staudte, M. Hattass, L. Spielberger, O. Jagutzki, V. Mergel, H. Schmidt-Böcking, G. Urbasch, H.W. Giessen, H. Bräuning, C.L. Cocke, M.H. Prior, R. Dörner, (2001), Optics Express, **8**, 368 – 376

27. A. Knapp, A. Kheifets, I. Bray, Th. Weber, A. L. Landers, S. Schössler, T. Jahnke, J. Nickles, S. Kammer, O. Jagutzki, L. Ph. Schmidt, T. Osipov, J. Rösch, M. H. Prior, H. Schmidt-Böcking, C. L. Cocke and R. Dörner, (2002), Phys. Rev. Lett., **89**, 033004-1

28. A. Knapp, M. Walter, Th. Weber, A.L. Landers, S. Schössler, T. Jahnke, M. Schöffler, J. Nickles, S. Kammer, O. Jagutzki, L. Ph. H. Schmidt, T. Osipov, J. Rösch, M. H. Prior, H. Schmidt-Böcking, C. L. Cocke, J. Feagin and R. Dörner, (2002), J. Phys. B: At. Mol. Opt. Phys., **235**, L521 – L526

29. R. Dörner,H. Schmidt-Bocking, T. Weber, T. Jahnke, M. Schoeffler, A. Knapp, M. Hattass, A. Czasch, L.Ph. Schmidt, O. Jagutzki, (2004), Radiation Physics and Chemistry, **70**, 191 – 206

30. L. Avaldi, and A. Huetz, (2005), J. Phys. B: At. Mol. Opt. Phys., **38**, 861

31. A. Knapp, A. Kheifets, I. Bray, Th. Weber, A. L. Landers, S. Schössler, T. Jahnke, J. Nickles, S. Kammer, O. Jagutzki, L. Ph. H. Schmidt, M. Schöffler, T. Osipov, M. H. Prior, H. Schmidt-Böcking, C. L. Cocke and R. Dörner, (2005), J. Phys. B: At. Mol. Opt. Phys., **38**, 615 – 633

32. A. Knapp, A. Kheifets, I. Bray, Th. Weber, A. L. Landers, S. Schössler, T. Jahnke, J. Nickles, S. Kammer, O. Jagutzki, L. Ph. H. Schmidt, M. Schöffler, T. Osipov, M. H. Prior, H. Schmidt-Böcking, C. L. Cocke and R. Dörner, (2005), J. Phys. B: At. Mol. Opt. Phys., **38**, 635 – 643

33. A. Knapp, B. Krässig, A. Kheifets, I. Bray, Th. Weber, A. L. Landers, S. Schössler, T. Jahnke, J. Nickles, S. Kammer, O. Jagutzki, L. Ph. H. Schmidt, M. Schöffler, T. Osipov, M. H. Prior, H. Schmidt-Böcking, C. L. Cocke and R. Dörner, (2005), J. Phys. B: At. Mol. Opt. Phys., **38**, 645 – 657

34. P. Bolognesi, V. Feyer, A. Kheifets, S. Turchini, T. Prosperi, N. Zema and L. Avaldi, (2008), J. Phys. B: At. Mol. Opt. Phys., **41**, 051003

35. M.S. Schoeffler, C. Stuck, M. Waitz, F. Trinter, T. Jahnke, U. Lenz, M. Jones, A. Belkacem, A. Landers, C. L. Cocke, J. Colgan, A. Kheifets, I. Bray, H. Schmidt-Boecking, R. Doerner, and Th. Weber, (2013), Phys. Rev. Lett., **111**, 013003

36. M. S. Schöffler, T. Jahnke, M. Waitz, F. Trinter, U. Lenz, C. Stuck, M. Jones, M. S. Pindzola, A. Belkacem, C. L. Cocke, A. Landers, J. Colgan, A. Kheifets, I. Bray, H. Schmidt-Böcking, R. Dörner and Th. Weber, (2014), Journal of Physics: Conference Series, **488**, 022007

37. R. Dörner, T. Weber, M. Achler, V. Mergel, L. Spielberger, O. Jagutzki, F. Afaneh, M.H. Prior, C.L. Cocke, H. Schmidt-Böcking, (2000), in: A.G. Suits, R.E. Continetti, Imaging in Chemical Dynamics, ACS Symposium Series **770**, Oxford University Press, 339-349

38. O. Jagutzki, A. Cerezo, A. Czasch, R. Dörner, M. Hattaß, M. Huang, V. Mergel, U. Spillmann, K. Ullmann-Pfleger, T. Weber, H. Schmidt-Böcking, G. D. W. Smith, (2002), IEEE Transactions on Nuclear Science, **49**, 2477 – 2483

39. H. Le Rouzo, (1986), J. Phys. B: At. Mol. Opt. Phys., **19**, L677-L682

40. H. Le Rouzo, (1988), Phys. Rev. A, **37**, 1512

41. J. M. Feagin, (1998), J. Phys. B: At. Mol. Opt. Phys., **31**, L729

42. A.S. Kheifets, (2005), Phys. Rev. A, **71**, 022704

43. A.S. Kheifets and Igor Bray, (2005), Phys. Rev. A, **72**, 022703

44. G. Dujardin, M. J. Besnard, L. Hellner, and Y. Malinovitch, (1987), Phys. Rev. A, **35**, 5012

45. H. Kossmann, O. Schwarzkopf, B. Kammerling, and V. Schmidt, (1989), Phys. Rev. Lett., **63**, 2040

46. T. J. Reddish, J. P. Wightman, M. A. MacDonald, and S. Cvejanovic, (1997), Phys. Rev. Lett., **79**, 2438

47. J. P. Wightman, S. Cvejanovic, and T. J. Reddish, (1998), J. Phys. B: At. Mol. Opt. Phys., **31**, 1753

48. N. Scherer, H. Lörch und V. Schmidt, (1998), J. Phys. B: At. Mol. Opt. Phys., **31**, L817

49. W. Vanroose, F. Martın, T. N. Rescigno, and C. W. McCurdy, (2005), Science, **310**, 1787

50. W. Vanroose, D. A. Horner, F. Martın, T. N. Rescigno, and C. W. McCurdy, (2006), Phys. Rev. A, **74**, 052702

51. D. A. Horner, W. Vanroose, T. N. Rescigno, F. Martın, and C. W. McCurdy, (2007), Phys. Rev. Lett., **98**, 073001

52. J. Colgan, M. S. Pindzola, and F. Robicheaux, (2007), Phys. Rev. Lett., **98**, 153001

53. T. J. Reddish, J. Colgan, P. Bolognesi, L. Avaldi, M. Gisselbrecht, M. Lavollee, M. S. Pindzola, and A. Huetz, (2008), Phys. Rev. Lett., **100**, 193001

54. L. Tao, C. W. McCurdy, and T. N. Rescigno, (2010), Phys. Rev. A, **82**, 023423

55. X. Guan, K. Bartschat, and B. I. Schneider, (2011), Phys. Rev. A, **83**, 043403

56. A. Ivanov and A. S. Kheifets, (2012), Phys. Rev. A, **85**, 013406

57. Wei-Chao Jiang, Liang-You Peng, Ji-Wei Geng, and Qihuang Gong, (2013), Phys. Rev. A, **88**, 063408

58. R. Dörner, H. Bräuning, O. Jagutzki, V. Mergel, M. Achler, R. Moshammer, J.M. Feagin, T. Osipov, A. Bräuning-Demian, L. Spielberger, J.H. McGuire, M.H. Prior, N. Berrah, J.D. Bozek, C.L. Cocke und H. Schmidt-Böcking, (1998), Phys. Rev. Lett., **81**, 5776 - 5779

59. S.A. Collins, A. Huetz, T.J. Reddish, D.P. Seccombe und K. Soejima, (2001), Phys. Rev. A, **64**, (2001), 062706

60. D.P. Seccombe, S.A. Collins, T.J. Reddish, P. Selles, L. Malegat, A.K. Kazansky und A. Huetz, (2002), J. Phys. B: At. Mol. Opt. Phys., **35**, (2002), 3767-3780

61. Th. Weber A. Czasch, O. Jagutzki, A. Müller, V. Mergel, A. Kheifets, J. Feagin, E. Rotenberg, G. Meigs, M. H. Prior, S. Daveau, A. L. Landers, C. L. Cocke, T. Osipov, H. Schmidt-Böcking, and R. Dörner, (2004), Phys. Rev. Lett., **92**, 163001-1

62. Th. Weber, A. O. Czasch, O. Jagutzki, A. K. Müller, V. Mergel, A. Kheifets, E. Rotenberg, G. Meigs, M. H. Prior, S. Daveau, A. Landers, C. L. Cocke, T. Osipov, R. Diez Muino, H. Schmidt-Böcking, R. Dörner, (2004), Nature, **Vol. 431**, 437 – 440, and Erratum: 2006, Nature, **Vol. 443**, 1014

63. M. Gisselbrecht, M. Lavollee, A. Huetz, P. Bolognesi, L. Avaldi, D. P. Seccombe, and T. J. Reddish, (2006), Phys. Rev. Lett., **96**, 153002

64. D. Akoury, K. Kreidi, T. Jahnke, Th. Weber, A. Staudte, M. Schöffler, N. Neumann, J. Titze, L. Ph. H. Schmidt, A. Czasch, O. Jagutzki, R. A. Costa Fraga, R. E. Grisenti, R. Díez Muiño, N. A. Cherepkov, S. K. Semenov, P. Ranitovic, C. L. Cocke, T. Osipov, H. Adaniya, J. C. Thompson, M. H. Prior, A. Belkacem, A. L. Landers, H. Schmidt-Böcking, R. Dörner, (2007), Science, **318**, 949 – 952

65. M. Gisselbrecht, M. Lavollée, A. Huetz, P. Bolognesi, L. Avaldi, D. P. Seccombe, and T. J. Reddish, (2007), Journal of Physics: Conference Series, **88**, 012006

66. K. Kreidi, D. Akoury, T. Jahnke, Th. Weber, A. Staudte, M. Schöffler, N. Neumann, J. Titze, L. Ph. H. Schmidt, A. Czasch, O. Jagutzki, R. A. Costa Fraga, R. E. Grisenti, M. Smolarski, P. Ranitovic, C. L. Cocke, T. Osipov, H. Adaniya, J. C. Thompson, M. H. Prior, A. Belkacem, A. L. Landers, H. Schmidt-Böcking, and R. Dörner, (2008), Phys. Rev. Lett., **100**, 133005-1 to 4

67. M. Schoeffler, K. Kreidi, D. Akoury, T. Jahnke, A. Staudte, N. Neumann, J. Titze, L. Ph. H. Schmidt, A. Czasch, O. Jagutzki, R. A. Costa Fraga, R. E. Grisenti, M. Smolarski, P. Ranitovic, C. L. Cocke, T. Osipov, H. Adaniya, S. Lee, J. C. Thompson, M. H. Prior, A. Belkacem, Th. Weber, A. Landers, H. Schmidt-Böcking, and R. Dörner, (2008), Phys. Rev. A, **78**, 013414-1 to 5

68. K. Kreidi, D. Akoury, T. Jahnke, Th. Weber, A. Staudte, M. Schöffler, N. Neumann, J. Titze, L.Ph.H. Schmidt, A. Czasch, O. Jagutzki, R.A. Costa Fraga, R.E. Grisenti, R. Díez Muiño, N.A. Cherepkov, S.K. Semenov, P. Ranitovic, C.L. Cocke, T. Osipov, H. Adaniya, J.C. Thompson, M.H. Prior, A. Belkacem, A. Landers, H. Schmidt-Böcking, and R. Dörner, (2009), Eur. Phys. J. Special Topics, **169**, 109-116

69. M. Waitz, D. Metz, J. Lower, C. Schober, M. Keiling, M. Pitzer, K. Mertens, M. Martins, J. Viefhaus, S. Klumpp, T. Weber, H. Schmidt-Böcking, L. Ph. H. Schmidt, F. Morales, S. Miyabe, T. N. Rescigno, C.W. McCurdy, F. Martín, J. B. Williams, M. S. Schöffler, T. Jahnke and R. Dörner, (2016), Physical Review Letters, **117**, 083002

70. L. Spielberger , O. Jagutzki, R. Dörner, J. Ullrich, U. Meyer, V. Mergel, M. Unverzagt, M. Damrau, T. Vogt, I. Ali, Kh. Khayyat, D. Bahr, H.G. Schmidt, R. Frahm, H. Schmidt-Böcking, (1995), Phys. Rev. Lett., **74**, 4615

71. L. Spielberger, O. Jagutzki, B. Krässig, U. Meyer, Kh. Khayyat, V. Mergel, Th. Tschentscher, Th. Buslaps, H. Bräuning, R. Dörner, T. Vogt, M. Achler, J. Ullrich, D.S. Gemmell, H. Schmidt-Böcking, (1996), Phys. Rev. Lett., **76**, 4685

72. L. Spielberger, H. Bräuning, A. Muthig, J.Z. Tang, J. Wang, Y. Qui, R. Dörner, O. Jagutzki, Th. Tschentscher, V. Honkimäki, V. Mergel, M. Achler, Th. Weber, Kh. Khayyat, J. Burgdörfer, J. McGuire, H. Schmidt-Böcking, (1999), Phys. Rev. A **59**, 371

73. Krässig, R.W. Dunford, D. S. Gemmell, S. Hasegawa, E. P. Kanter, H. Schmidt-Böcking, W. Schmitt, S. H. Southworth, Th. Weber, and L. Young, (1999), Phys. Rev. Lett, **83**, 53 – 56

74. F. Maulbetsch and J. S. Briggs, (1995), J. Phys. B: At. Mol. Opt. Phys., **28**, 551

75. M. Walter, A. Meremianin, and J. S. Briggs, (2003), Phys. Rev. Lett., **90**, 233001

76. M. Walter, A. V. Meremianin, and J. S. Briggs, (2003), J. Phys. B: At. Mol. Opt. Phys., **36**, 4561

77. F. Martin, J. Fernández, T. Havermeier, L. Foucar, Th. Weber, K. Kreidi, M. Schöffler, L. Schmidt, T. Jahnke, O. Jagutzki, A. Czasch, E. P. Benis, T. Osipov, A. L. Landers, A. Belkacem, M. H. Prior, H. Schmidt-Böcking, C. L. Cocke, R. Dörner, (2007), Science, **315**, 629 – 633

78. Jorge Fernández and Fernando Martín, (2009), New Journal of Physics, **11**, 043020

79. M. Schoeffler, J. Titze, N. Petridis, T. Jahnke, K. Cole, L. Ph. H. Schmidt, A. Czasch, D. Akoury, O. Jagutzki, J. B. Williams, N. A. Cherepkov, S. K. Semenov, C. W. McCurdy, T. N. Rescigno, C. L. Cocke, T. Osipov, S. Lee, M. H. Prior, A. Belkacem, A. L. Landers, H. Schmidt-Böcking, Th. Weber, R. Dörner, (2008), Science, **320**, 920 – 923

80. M.S. Schoeffler, T. Jahnke, J. Titze, N. Petridis, K. Cole, L. Ph. H. Schmidt, A. Czasch, O. Jagutzki, J.B. Williams, C. L. Cocke, T. Osipov, S. Lee, M.H. Prior, A. Belkacem, A.L. Landers, H. Schmidt-Boecking, R. Doerner, and Th. Weber, (2011), New Journal of Physics, **13**, special edition: matter wave optics, 095013

81. N.A. Cherepkov, S.K. Semenov, M. S. Schöffler, J. Titze, N. Petridis, T. Jahnke, K. Cole, L. Ph. H. Schmidt, A. Czasch, D. Akoury, O. Jagutzki, J. B. Williams, C. L. Cocke, T. Osipov, S. Lee, M. H. Prior, A. Belkacem, A. L. Landers, H. Schmidt-Böcking, Th. Weber, and R. Dörner, (2009), Phys. Rev. A, **80**, 051404(R)

82. S.K. Semenov, M. S. Schöffler, J. Titze, N. Petridis, T. Jahnke, K. Cole, L. Ph. H. Schmidt, A. Czasch, D. Akoury, O. Jagutzki, J. B. Williams, T. Osipov, S. Lee, M. H. Prior, A. Belkacem, A. L. Landers, H. Schmidt-Böcking, Th. Weber, N. A. Cherepkov, and R. Dörner, (2010), Phys. Rev. A, **81**, 043426

83. N.A. Cherepkov, S.K. Semenov, M.S. Schöffler, J. Titze, N. Petridis, T. Jahnke, K. Cole, L.Ph.H. Schmidt, A. Czasch, D. Akoury, O. Jagutzki, J.B. Williams, T. Osipov, S. Lee, M.H. Prior, A. Belkacem, A.L. Landers, H. Schmidt-Böcking, R. Dörner, and Th. Weber, (2010), Phys. Rev. A, **82**, 023420

84. B. Gaire, D. J. Haxton, F. P. Sturm, J. Williams, A. Gatton, I. Bocharova, N. Gehrken, M. Schöffler, H. Gassert, S. Zeller, J. Voigtsberger, T. Jahnke, M. Zohrabi, D. Reedy, C. Nook, A. L. Landers, A. Belkacem, C. L. Cocke, I. Ben-Itzhak, R. Dörner, and Th. Weber, (2015), Phys. Rev. A, **92**, 013408

85. M. Waitz, D. Aslituerk, N. Wechselberger, H.K. Gill, J. Rist, F. Wiegandt, C. Goihl, G. Kastirke, M. Weller, T. Bauer, D. Metz, F.P. Sturm, J. Voigtsberger, S. Zeller, F. Trinter, G. Schiwietz, T. Weber, J.B. Williams, M.S. Schoeffler, L.Ph.H. Schmidt, T. Jahnke, and R. Doerner, (2016), Phys. Rev. Lett., **116**, 043001

86. R. Doerner, V. Mergel, O. Jagutzki, L. Spielberger, J. Ullrich, R. Moshammer, and H. Schmidt-Boecking, (2000), Phys. Rep., **330**, 95

87. J. Ullrich, R. Moshammer, A. Dorn, R.Doerner, L. P. H. Schmidt, and H. Schmidt-Boecking, (2003), Rep. Prog. Phys. **66**, 1463

88. T. Jahnke, T. Weber, T. Osipov, A. L. Landers, O. Jagutzki, L. P. H. Schmidt, C. L. Cocke, M.H. Prior, H. Schmidt-Boecking, and R. Doerner, (2004), J. Electron Spectrosc. Relat. Phenom. **141**, 229

89. L. Foucar, Dissertation, (2008), University of Frankfurt, Department of Physics, “Auslese von Delaylinedetektoren mit Hilfe von Transientenrekordern”

90. R. N. Zare, J. Chem. Phys., (1967), **47**, 204

91. R. N. Zare, Mol. Photochem., (1972), **4**, 1

92. T. Osipov, C. L. Cocke, M. H. Prior, A. Landers, T. Weber, O. Jagutzki, L. Schmidt, H. Schmidt-Böcking and R. Dörner, (2003), Phys. Rev. Lett., **90**, 233002-1

93. Th. Weber, M. Weckenbrock, M. Balser, L. Schmidt, O. Jagutzki, W. Arnold, O. Hohn, M. Schöffler, E. Arenholz, T. Young, T. Osipov, L. Foucar, A. De Fanis, R. Diez Muino, H. Schmidt-Böcking, C. L. Cocke, M. H. Prior, and R. Dörner, (2003), Phys. Rev. Lett., **90**, 153003-1

94. T. Osipov, A. S. Alnaser, S. Voss, M. H. Prior, T. Weber, O. Jagutzki, L. Schmidt, H. Schmidt-Böcking, R. Dörner, A. Landers, E. Wells, B. Shan, C. Maharjan, B. Ulrich, P. Ranitovic, X. M. Tong, C. D. Lin and C. L. Cocke, (2005), J. of Mod. Opt., **52**, No. 2-3, 439 – 451

95. G. Dawber, L. Avaldi, A.G. McConkey, H. Rojas, M.A. MacDonald und G.C. King, J. Phys. B: At. Mol. Opt. Phys., **28**, (1995), L271

96. L. Malegat, P. Selles und A. Huetz, J. Phys. B: At. Mol. Opt. Phys., **30,** (1997), 251-261

97. L. Malegat, P. Selles, P. Lablanquie, J. Mazeau und A. Huetz, J. Phys. B: At. Mol. Opt. Phys., **30,** (1997), 263-276

98. O. Schwarzkopf und V. Schmidt, J. Phys. B: At. Mol. Opt. Phys., **28**, (1995), 2847

99. C. Dawson, S. Cvejanovic, D.P. Seccombe, T.J. Reddish, F. Maulbetsch, A. Huetz , J. Mazeau und A.S. Kheifets, J. Phys. B: At. Mol. Opt. Phys, **34**, (2001), L525-533

100. T.J. Reddish und J.M. Feagin, J. Phys. B: At. Mol. Opt. Phys., **32**, (1999), 2473-2486

101. R. Diez Muino , D. Rolles, F.J. Garcia de Abajo, F. Starroste, W. Schattkee, C.S. Fadley , M.A. Van Hove, Journal of Electron Spectroscopy and Related Phenomena, (2001), **114–116**, 99–105

102. J. M. Feagin, J. Colgan, A. Huetz, and T. J. Reddish, (2009), Phys. Rev. Lett., **103**, 033002

Figures

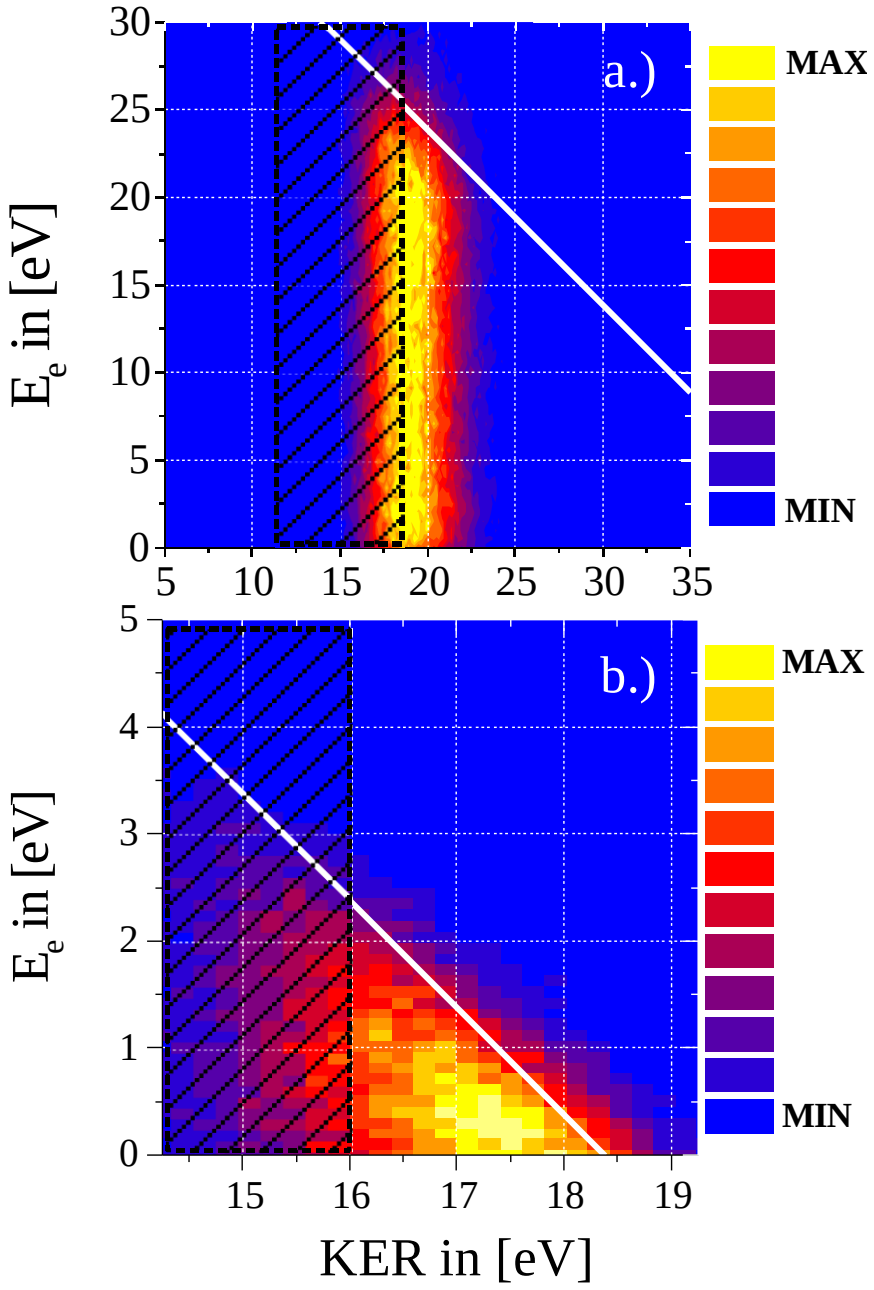

Figure 1: Energy phase space of the photo double ionization of deuterium (a) and hydrogen (b) molecules. The energy of one electron as a function of the Kinetic Energy Release KER is plotted for two different photon energies a.) 75 eV and b.) 50 eV. The white (color online) diagonals indicate energy conservation e.g. constant sum energy of all four particles. The hatched areas represent the cuts made for Figures 2. In b.) electrons below 1 eV were chosen for Figure 3 and 8 eliminating effects due to a constricted phase space by the KER.

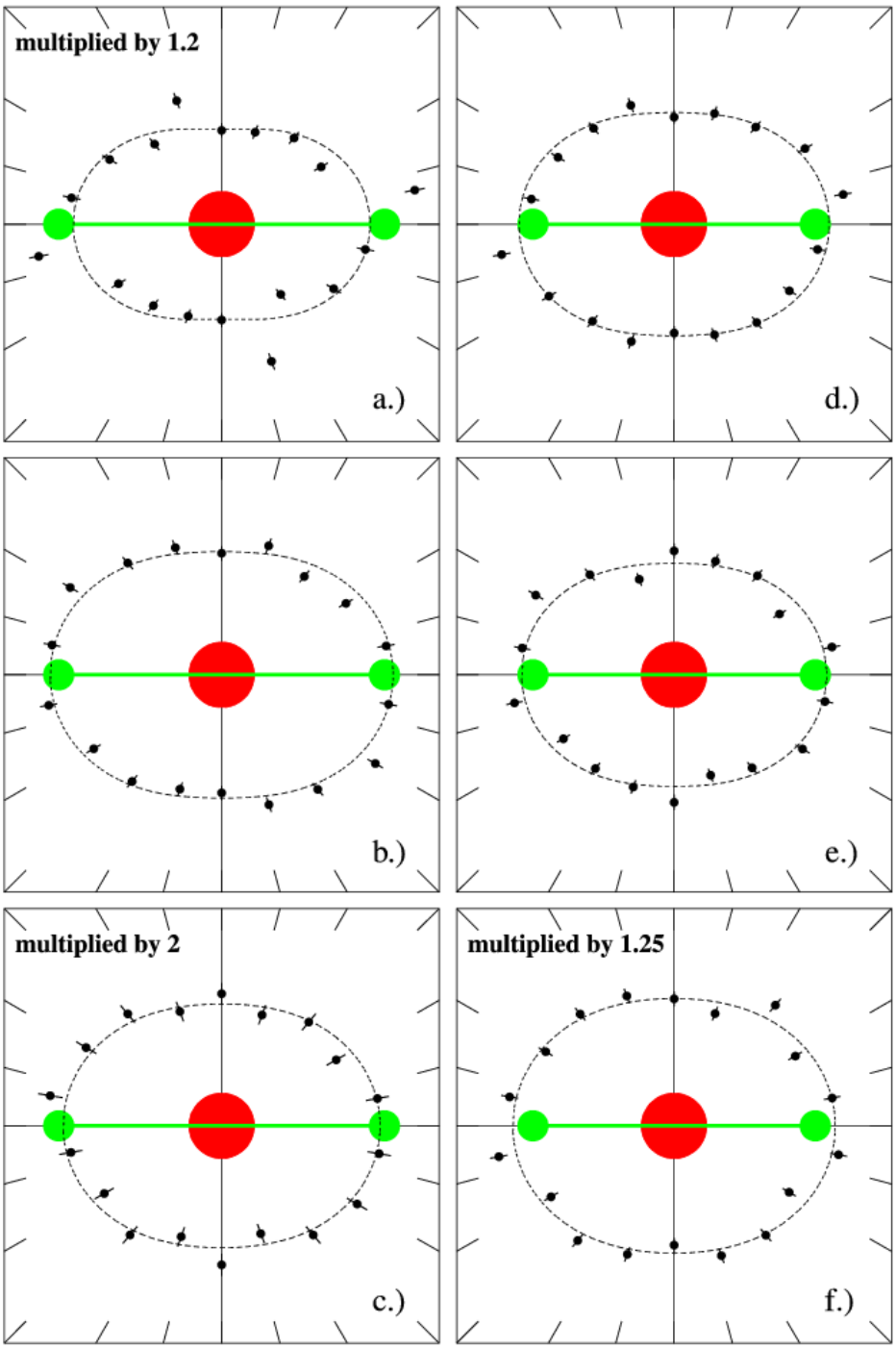

Figure 2: Azimuthal angular electron distributions of the full fragmentation of hydrogen (a-c: 50 eV photon energy) and deuterium (d-f: 75 eV photon energy) molecules for different electron energies E_{e1}. The left and right columns are each internormalized. The data have been multiplied by the factors indicated in the spectra for better comparison. The polarization vector of the incoming light ε is parallel to the normal of the paper plane (±30 degree). The molecular axis lies horizontally (±10 degree) as indicated by the green barbell (color online). The data have been integrated over the orientation of the second electron, as indicated by the full red circles (color online). Small and similar KER intervals e.g. large internuclear separations were chosen to avoid KER constraints and, in comparison with an isotropic emission for the photo double ionization of helium, assure the most possible break in symmetry. The KER interval in the left column (a-c) is 12 to 16 eV. The KER interval in the right column (d-f) is 12 to 18 eV. The electron energy intervals are as follows: (a) 0 to 1 eV, (b) 1 to 2.5eV, (c) 2.5 to 5.5 eV, (d) 0 to 5.5 eV, (e) 10 to 15 eV, and (f) 12 to 18 eV. The dashed lines show a fit $[1+\beta(E)\cdot(3/2\cdot \cos^2\theta - 1/2)]$ to guide the eye.

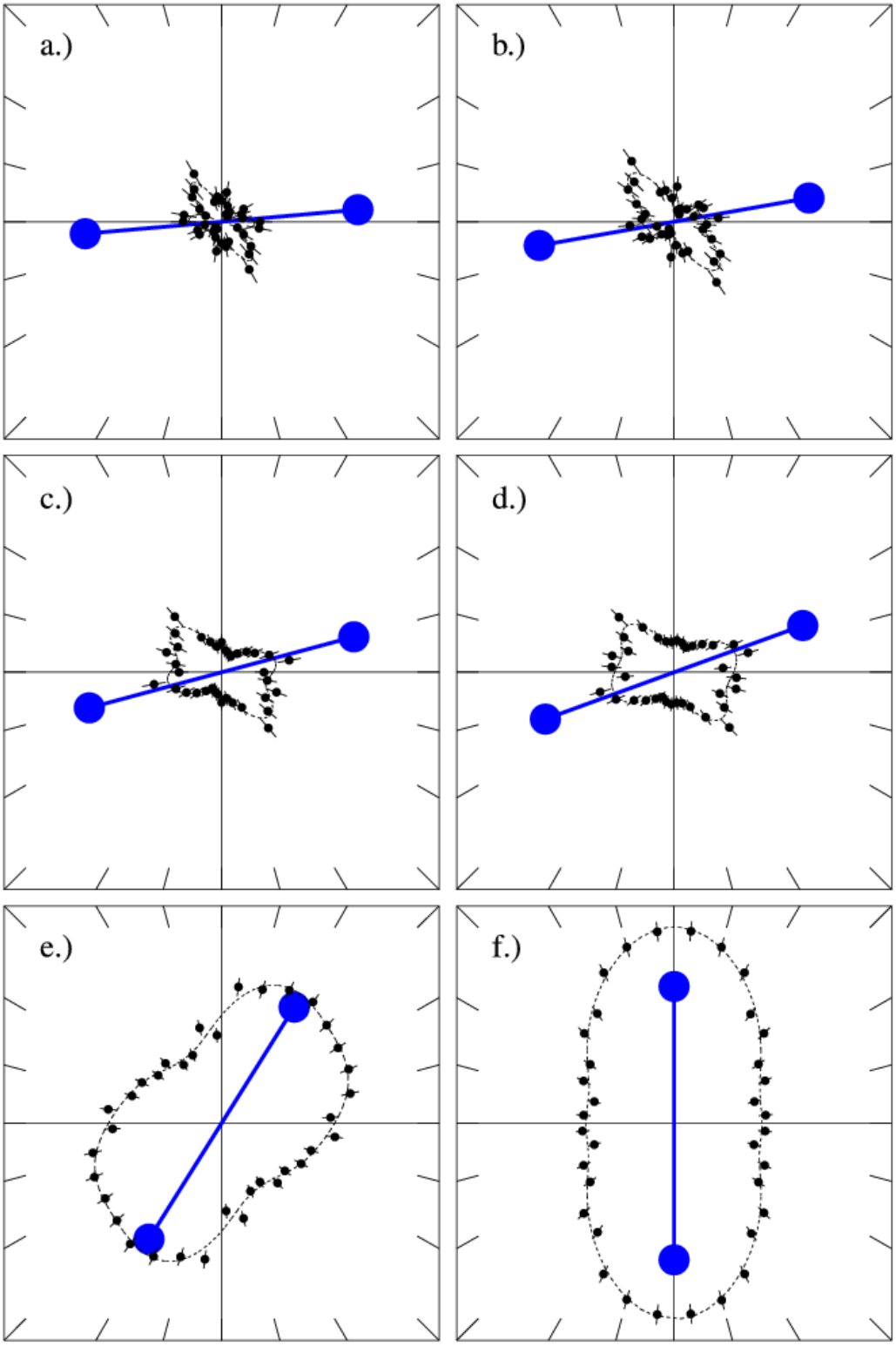

Figure 3: Polar angular distributions of one electron for the photo double ionization of hydrogen molecules at 50 eV as a function of the molecular orientation (±12 degree). The molecular axis (blue barbell, color online) and the polarization vector ε (which lies horizontally) span a plane. The emission pattern of one of the two low energy electrons (0 to 1 eV) is plotted with an acceptance angle of ±20 degree in this plane. The data are integrated over the Kinetic Energy Release (KER) and the second electron. The spectra are internormalized. The dashed lines show a fit with spherical harmonics ($l \in [1,4]$, $m \in [0,1]$).

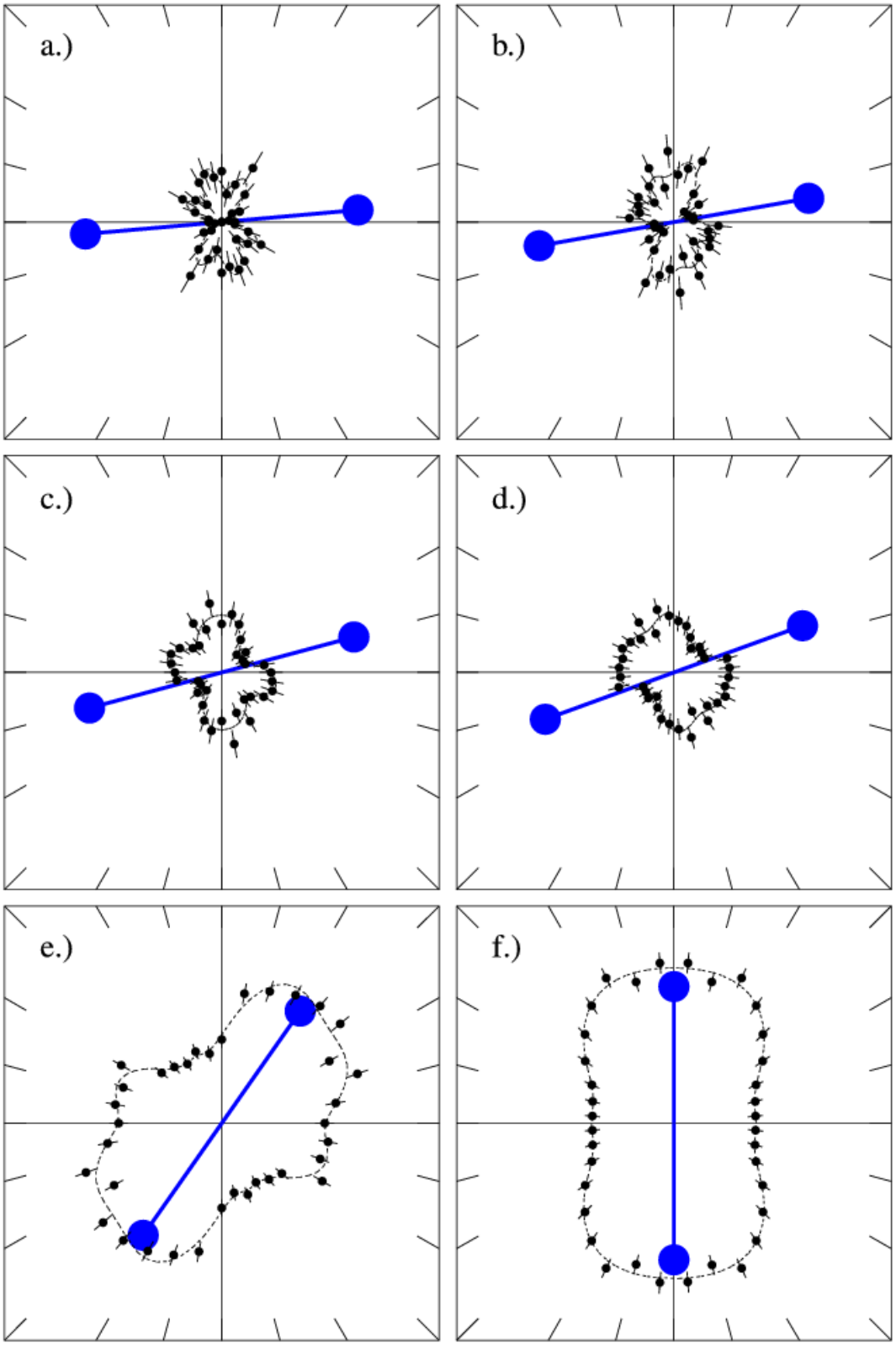

Figure 4: Polar angular distributions of one electron for the photo double ionization of deuterium molecules at 75 eV as a function of the molecular orientation (±12 degree). The molecular axis (blue barbell, color online) and the polarization vector ε (which lies horizontally) span a plane. The emission pattern of the low energy electron (0 to 3 eV) is plotted with an acceptance angle of ±20 degree in this plane. The data are integrated over the Kinetic Energy Release (KER) and the second electron. The spectra are internormalized. The dashed lines show a fit with spherical harmonics ($l \in [1,4]$, $m \in [0,1]$).

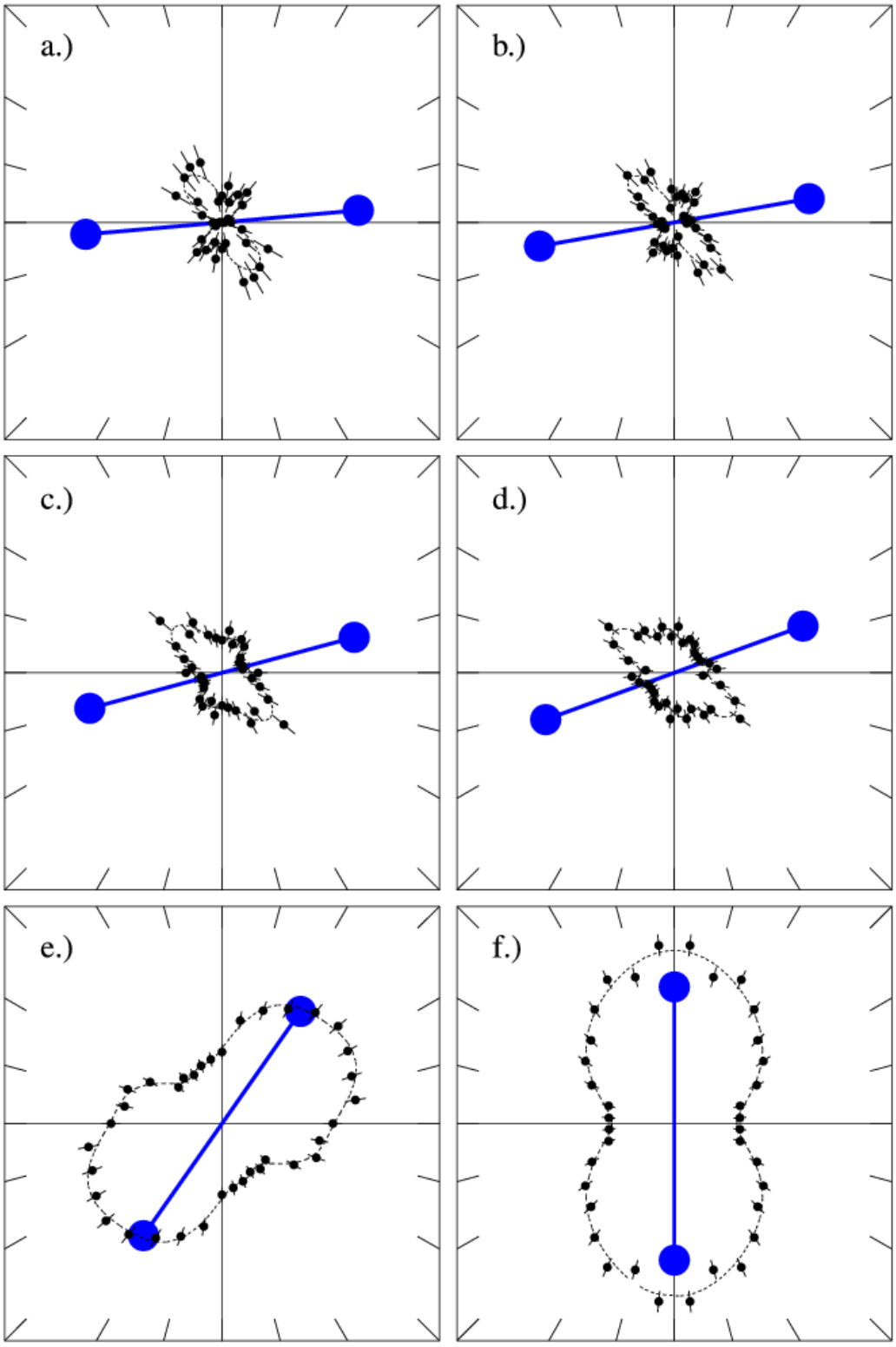

Figure 5: Polar angular distributions of one electron for the photo double ionization of deuterium molecules at 75 eV as a function of the molecular orientation (±12 degree). The molecular axis (blue barbell, color online) and the polarization vector ε (which lies horizontally) span a plane. The emission pattern of one of the two electrons (11 to 14 eV) is plotted with an acceptance angle of ±20 degree in this plane. The data are integrated over the Kinetic Energy Release (KER) and the second electron. The spectra are internormalized. The dashed lines show a fit with spherical harmonics (l ∈ [1,4], m ∈ [0,1]).

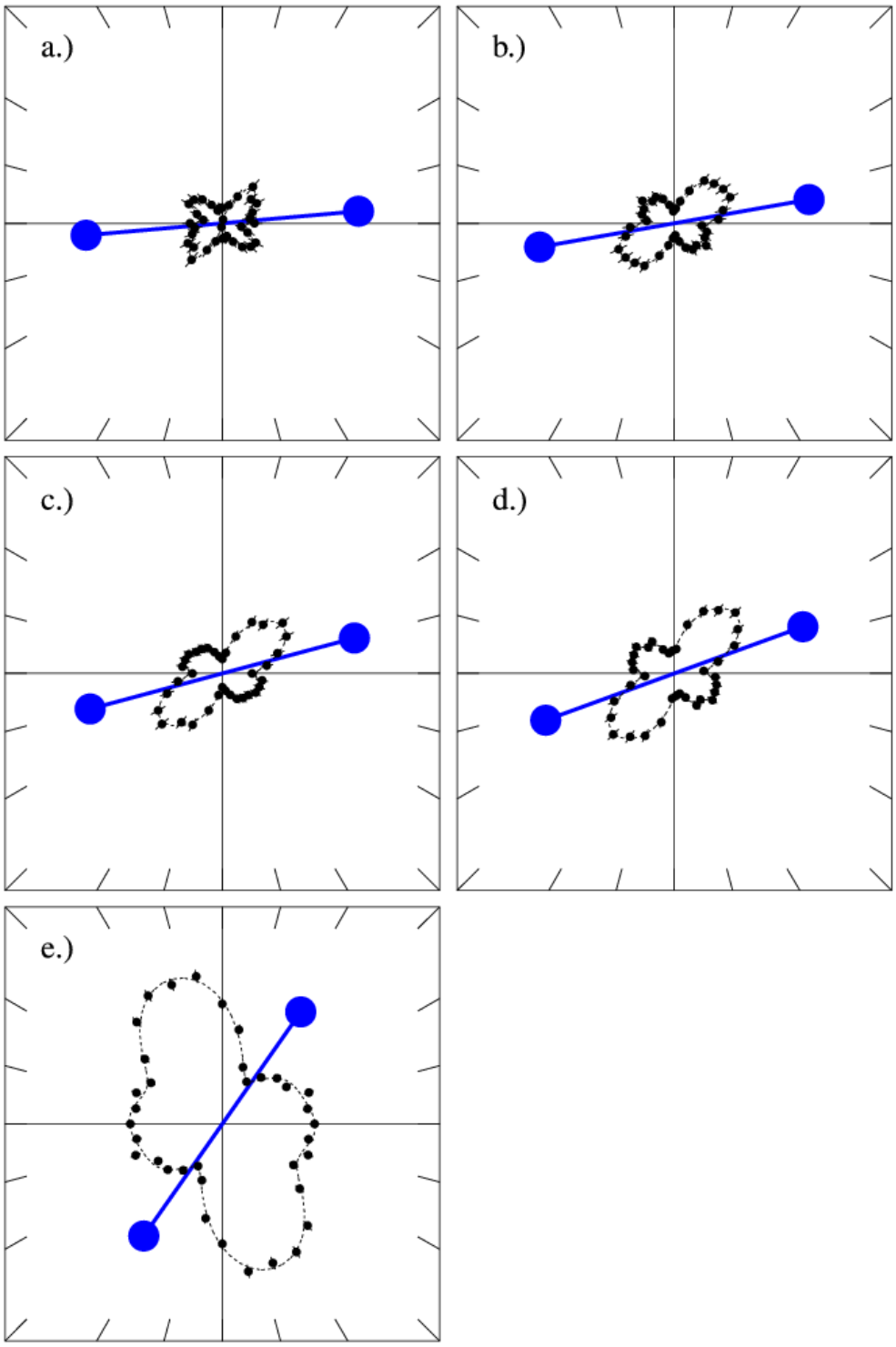

Figure 6: Polar angular distributions of one electron for the photo double ionization of deuterium molecules at 75 eV as a function of the molecular orientation (±12 degree). The molecular axis (blue barbell, color online) and the polarization vector ε (which lies horizontally) span a plane. The emission pattern of the high energy electron (> 19.5 eV) is plotted with an acceptance angle of ±20 degree in this plane. The data are integrated over the Kinetic Energy Release (KER) and the second electron. A pure Σ-Π-transition (e.g. molecular axis at 90 degree) is not shown here due to multi-hit problems on the detector. The spectra are internormalized. The dashed lines show a fit with spherical harmonics (l ∈ [1,4], m ∈ [0,1]).

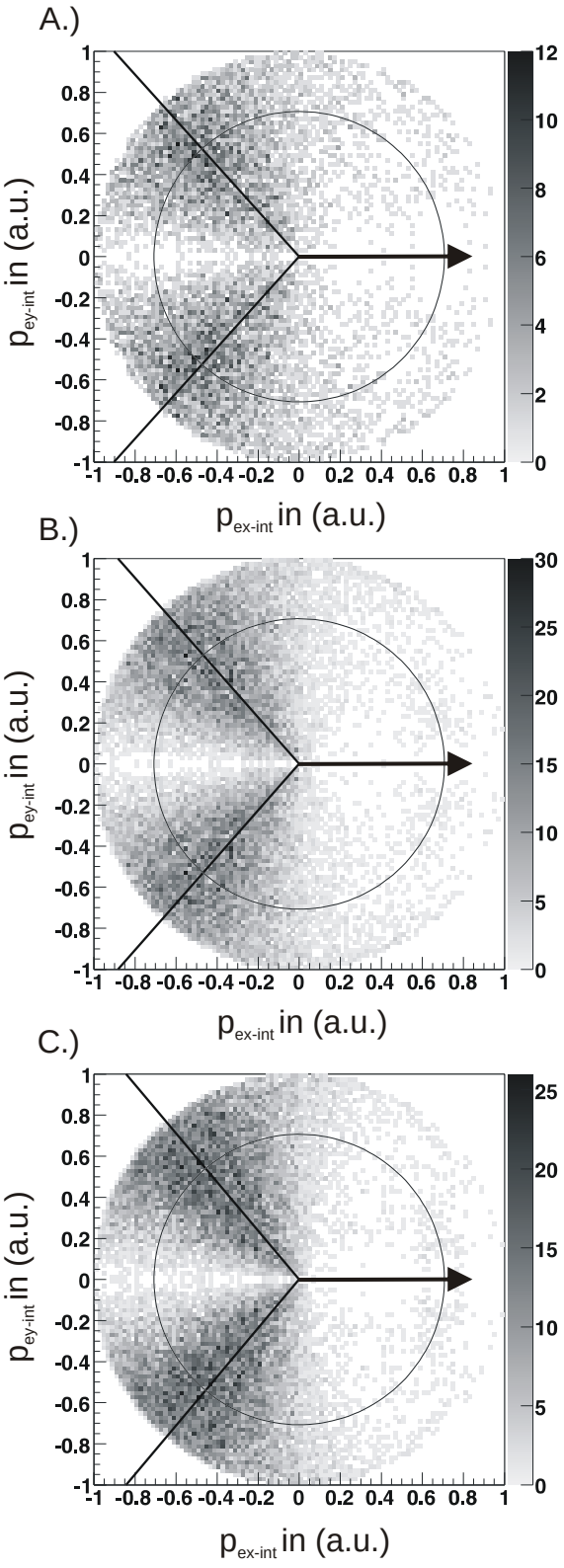

Figure 7: Relative electron-electron momentum distributions of the photo double ionization of hydrogen molecules at 50 eV. The internal plane is spanned by the two emitted electrons with one always going to the right as indicated by the black arrow (the length of the arrow has no meaning). The displayed momentum distribution is normalized to 1 for better comparison. The electron sum energy is limited from (A) 0 to 1 eV, (B) 1 to 2 eV, and (C) 2 to 3 eV. The distributions are integrated over all orientations of the polarization directions and the molecular axis. The circles indicate equal energy sharing between the two electrons. The diagonals represent the mean relative angles between the two electrons.

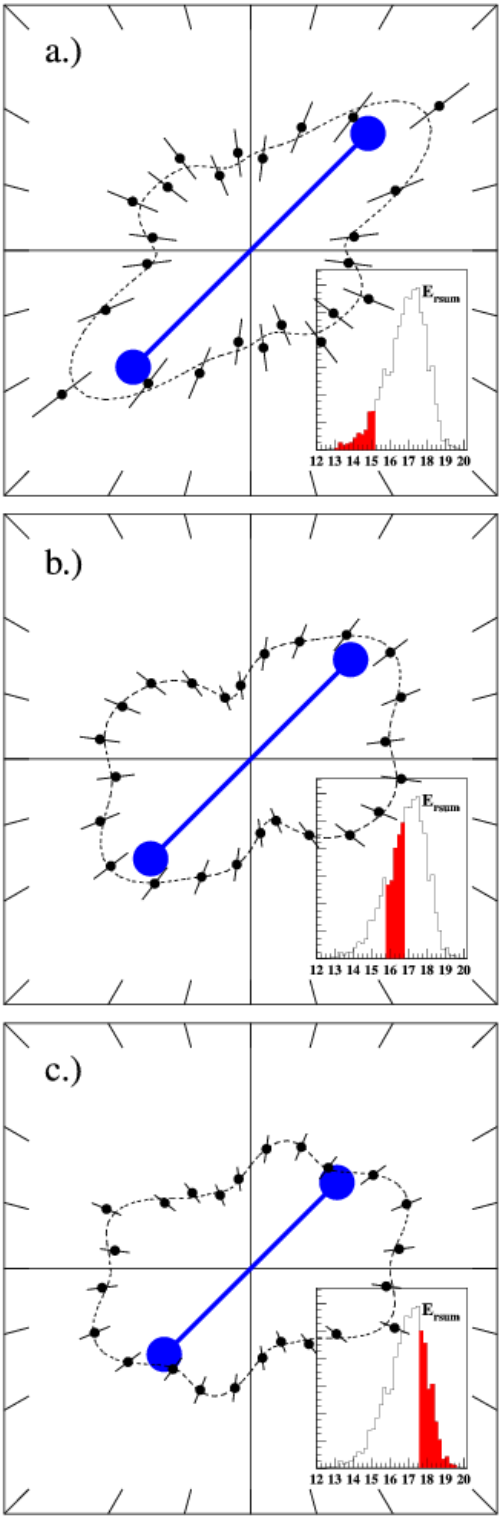

Figure 8: Polar angular distributions of one electron for the photo double ionization of hydrogen molecules at 50 eV as a function of the Kinetic Energy Release KER (see insets). The molecular axis at a fixed orientation (blue barbell at 45±15 degree, color online) and the polarization vector ε (which lies horizontally) span a plane. The emission pattern of one of the two low energy electrons (0 to 1 eV) is plotted with an acceptance angle of ±25 degree in this plane. The orientation of the molecular axis represents a mix of Σ and Π transitions. The data are integrated over the second electron. The cross sections are normalized to the chosen KER intervals as seen in the insets. The dashed lines show a fit with spherical harmonics ($l \in [1,4]$, $m \in [0,1]$).

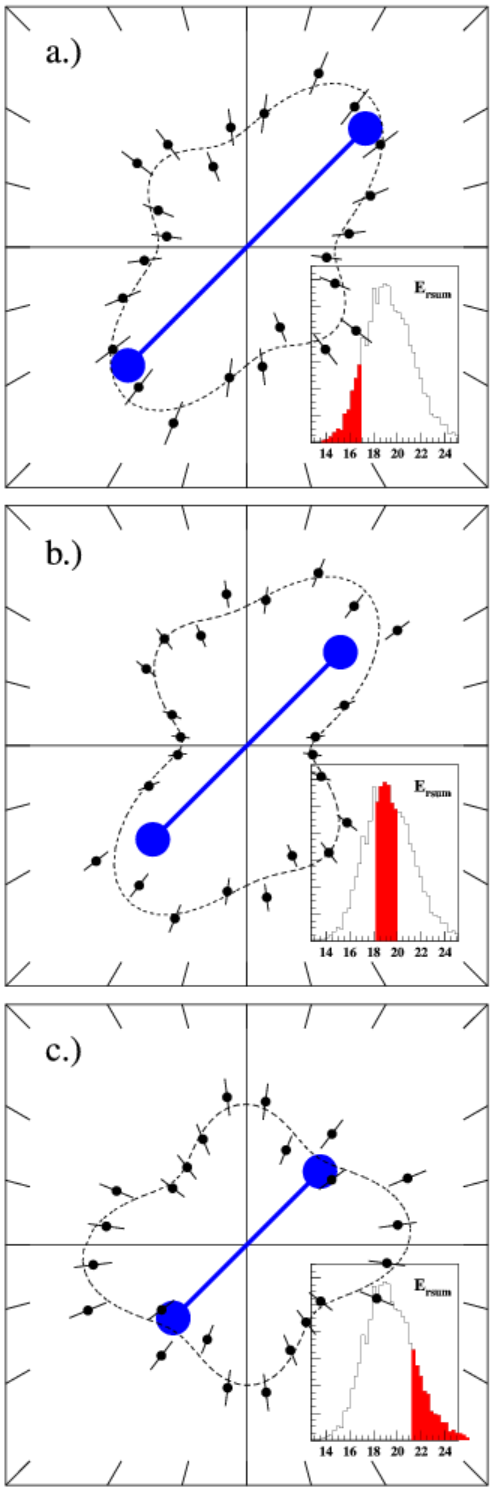

Figure 9: Polar angular distributions of one electron for the photo double ionization of deuterium molecules at 75 eV as a function of the Kinetic Energy Release KER (see inset). The molecular axis at a fixed orientation (blue barbell at 45±15 degree, color online) and the polarization vector ε (which lies horizontally) span a plane. The emission pattern of the low energy electron (0 to 5.5 eV) is plotted with an acceptance angle of ±25 degree in this plane. The orientation of the molecular axis represents a mix of Σ and Π transitions. The data are integrated over the second electron. The cross sections are normalized to the chosen KER intervals as seen in the insets. The dashed lines show a fit with spherical harmonics ($l \in [1,4]$, $m \in [0,1]$).

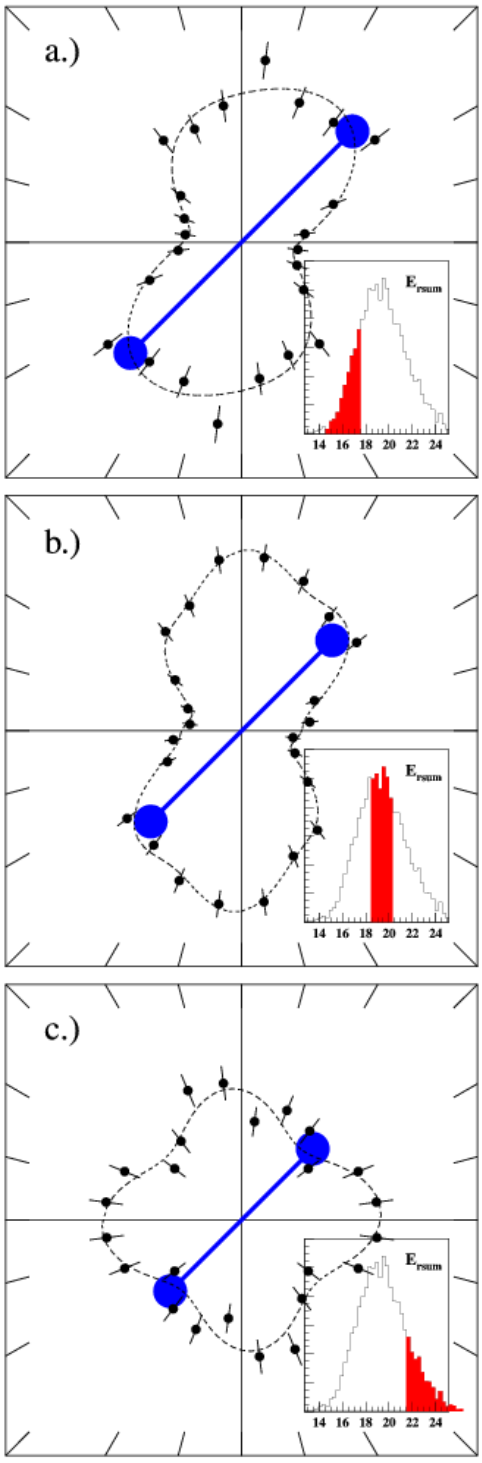

Figure 10: Polar angular distributions of one electron for the photo double ionization of deuterium molecules at 75 eV as a function of the Kinetic Energy Release KER (see insets). The molecular axis at a fixed orientation (blue barbell at 45±15 degree, color online) and the polarization vector ε (which lies horizontally) span a plane. The emission pattern of one of the two electrons (10 to 15 eV) is plotted with an acceptance angle of ±25 degree in this plane. The orientation of the molecular axis represents a mix of Σ and Π transitions. The data are integrated over the second electron. The cross sections are normalized to the chosen KER intervals as seen in the insets. The dashed lines show a fit with spherical harmonics ($l \in [1,4]$, $m \in [0,1]$).

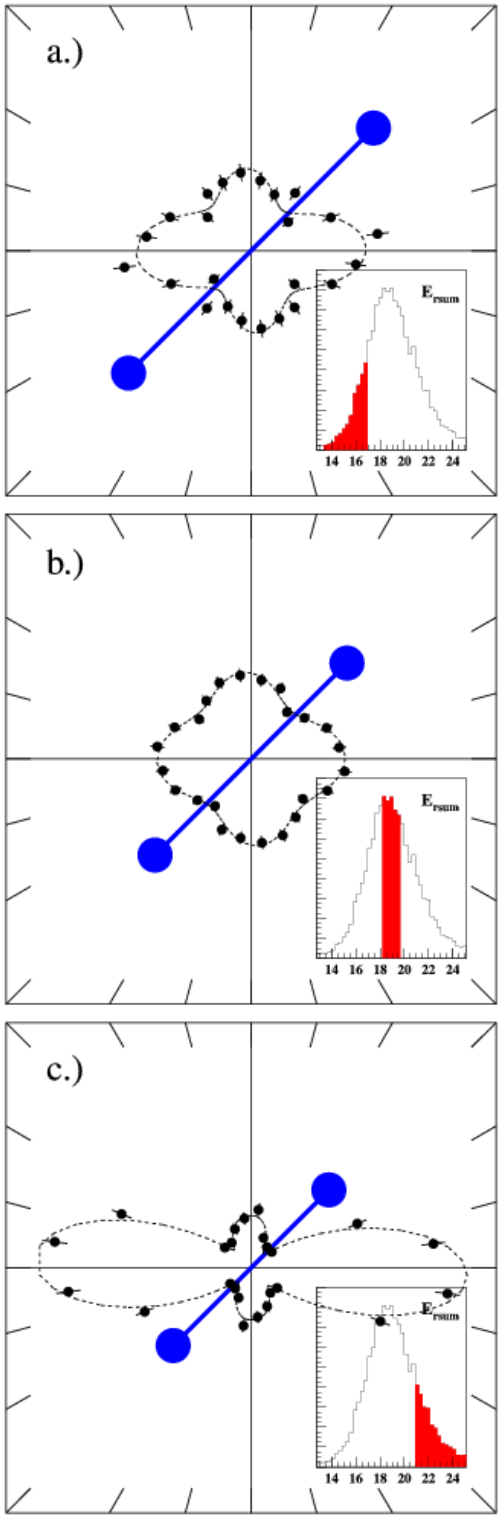

Figure 11: Polar angular distributions of one electron for the photo double ionization of deuterium molecules at 75 eV as a function of the Kinetic Energy Release KER (see insets). The molecular axis at a fixed orientation (blue barbell at 45±15 degree, color online) and the polarization vector ε (which lies horizontally) span a plane. The emission pattern of the high energy electron (> 19.5 eV) is plotted with an acceptance angle of ±25 degree in this plane. The orientation of the molecular axis represents a mix of Σ and Π transitions. The data are integrated over the second electron. The cross sections are normalized to the chosen KER intervals as seen in the insets. The dashed lines show a fit with spherical harmonics ($l \in [1,4]$, $m \in [0,1]$).